RSC Advances

PAPER

View Article Online
View Journal | View Issue

Cite this: *RSC Adv.*, 2020, **10**, 27424

NiFe LDH/CuO nanosheet: a sheet-on-sheet strategy to boost the active site density towards oxygen evolution reaction†

Benfeng Lin,[ab] Huafeng le,[ab] Feng Xu *[ab] and Shichun Mu *[c]

Received 2nd April 2020
Accepted 25th June 2020

DOI: 10.1039/d0ra02985h

rsc.li/rsc-advances

The amount of active sites of a catalyst is of great importance to enhance the oxygen evolution reaction (OER) activity. Here, the sheet-on-sheet strategy is proposed to effectively increase the density of active sites of NiFe layered double hydroxide (NiFe LDH) catalyst in terms of structural engineering. As a non-precious electrocatalyst for the OER, NiFe LDH is grown directly on CuO nanosheets. As a result, the received NiFe LDH/CuO nanosheet catalyst with sheet-on-sheet structure shows an ultralow overpotential of 270 mV at 20 mA cm^{-2}, much lower than that of RuO_2 as a benchmark. The CuO nanosheets, as substrate, play the vital role in downsizing the NiFe LDH, leading to the raised active site density.

Electrochemical water splitting is an important technique for facile energy storage and transfer.[1] The oxygen evolution reaction (OER), as a half reaction of water splitting, suffers from sluggish kinetics due to the complicated charge transfer process.[3] As a result, a larger overpotential is required to drive the OER process. Relative to the state-of-the-art noble metal catalysts, such as RuO_2 and IrO_2, reliable non-precious electrocatalysts are urgently needed to boost the OER activity and reduce the cost.[4]

Currently, mixed NiFe layered double hydroxide (NiFe LDH) electrocatalysts exhibit favourable intrinsic OER activities.[1–3] However, restriction on applications of NiFe LDH lies in the limited electrochemically active surface area and low conductivity.[4] Some strategies, such as defect engineering,[5–7] and NiFe based ternary LDH,[8] have been proposed for enhancing the OER activity. Recent studies have shown that the OER activity of NiFe LDH can be further enhanced by structure engineering.[8,9] Especially, NiFe LDH with 3D architecture provides large specific surface area and sufficient active catalytic reaction sties.[10–12] The substrate used for growing the NiFe LDH is important to construct the 3D architecture. However, the substrates, such Ni/Cu foam,[13,14] and porous carbon,[15,16] are commonly in the size scale of micro- or even centi-meter, and leads to the large size of NiFe LDH, which undermines the activity. Hence, downsizing the substrate is essential for decreasing the size of NiFe LDH and improving the catalytic activity. Bin *et al.* fabricated the NiFe LDH on AgNWs with heterointerfaces which optimized the electronic structures and boost the OER activity.[17] Zhou *et al.* deposited the NiFe LDH on CuO nanorods to construct a core–shell heterostructure, which demonstrated the overpotential of 290 mV at 50 mA cm^{-2} in 1 M KOH.[18] Zhang *et al.* deposited the NiFe LDH on NiCoP nanoarray, the resulting electrode required the overpotential of 220 mV to deliver 10 mA in 1 M KOH.[19] 1D nano-structure with NiFe LDH directly growing on nanowires seems to be effective for support engineering.

Herein, we explore a sheet-on-sheet structure of NiFe LDH catalyst for enhancing the OER activity. We first grow CuO nanosheets (CuO NSs) on Cu nanowires (Cu NWs), then deposit NiFe LDH on CuO NSs, constructing a NiFe LDH/CuO NS structure. The CuO NS offers the nano-sized substrate for NiFe LDH growth, and enhance the number of active sites, thus greatly improving the OER performance of catalysts.

The as-prepared Cu NWs with the smooth surface (Fig. S1†) were used as templates. XRD shows the typical Cu diffraction with peaks at 2θ of 43.3°, 50.4°, and 74.1°, corresponding to (111), (200), and (220) facets (JCPDS 04-0836), respectively (Fig. 1). After treated in NaOH solutions, the leaf-like nanosheets were grown perpendicularly and homogeneously on the surface of CuNWs at high density (Fig. S1†). These nanosheets are in the triangle shape and have the 2D size of around 200 nm. The diffraction peaks at 35.5°, 38.7°, 48.7°, 58.3°, 61.5°, 66.2° and 67.9° belong to (002), (111), (−202), (202), (−113), (311), and (113) facets of CuO (JCPDS 45-0937), respectively, illustrating the nanosheets consists of CuO. With the formation of NiFe

[a]College of Materials Science and Engineering, Fuzhou University, Fuzhou 350108, P. R. China. E-mail: xufeng.mater@fzu.edu.cn

[b]Key Laboratory of Eco-materials Advanced Technology, Fuzhou University, 350108, P. R. China

[c]State Key Laboratory of Advanced Technology for Materials Synthesis and Processing, Wuhan University of Technology, Wuhan 430070, P. R. China. E-mail: msc@whut.edu.cn

† Electronic supplementary information (ESI) available. See DOI: 10.1039/d0ra02985h

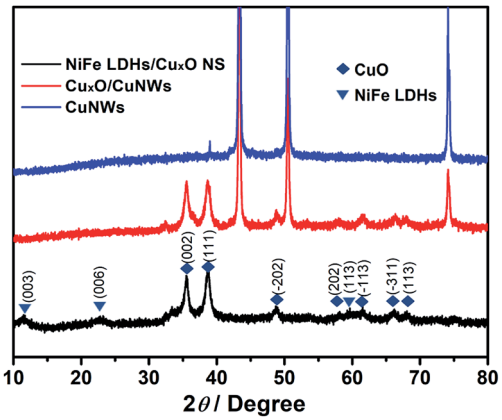

Fig. 1 XRD pattern of CuNWs, CuO/CuNWs, and NiFe LDH/CuO NS.

LDH, Cu diffraction signals disappear, due to the reaction of Cu with the ammonia and final dissolution. The peaks at 11.4°, 23.4°, and 59.8° correspond to the (003), (006), and (113) facets of NiFe LDH (JCPDS 40-0215). The XRD results show that the final composition of the as-prepared catalyst is NiFe LDH/CuO NS.

The SEM image reveals the remaining of nanowire shape even after removal of CuNWs (Fig. 2). High density of very thin NiFe LDH can be observed. NiFe LDH has the 2D size of around 100 nm. The homogeneous dispersion of O, Cu, Ni and Fe elements can be detected in NiFe LDH/CuO NS. The mass ratio of Cu, O, Ni, and Fe detected by EDS is shown in Table S1,† the Ni : Fe atomic ratio is close to 4 : 1. NiFe LDH directly grown on CuNWs with different dosages of Ni and Fe precursors (NiFe LDH/CuNWs-L, NiFe LDH/CuNWs, and NiFe LDH/CuNWs-H) were also prepared for comparison. NiFe LDH is found on NiFe LDH/CuNWs-L and NiFe LDH/CuNWs with a low density (Fig. S2†). NiFe LDH/CuNWs-L shows NiFe LDH with very small size. As the dosage of Ni and Fe precursors rises (LDH/CuNWs-H), both the density and the size of NiFe LDH increase. The size of NiFe LDH becomes large and even reaches one micrometer. The difference in the morphologies of NiFe LDH/CuO NS and NiFe LDH/CuNWs demonstrates that the CuO nanosheets, as nano-sized substrate, are crucial for the morphology engineering of NiFe LDH. A control experiment with different NiFe dosages but the same amount of support was also carried out (Fig. S3†). The density of NiFe LDH becomes bushier as NiFe dosage increases.

The composition and valence information were surveyed by XPS (Fig. 3). Fig. 3A shows the Cu 2p orbital. The peaks at around 934 and 953 eV are ascribed to Cu $2p_{3/2}$ and $2p_{1/2}$, respectively. The satellite peaks in the range of 938–947 eV relate to Cu^{2+}.[20] The peaks of Fe 2p at 712.5 and 724.6 eV (Fig. 3B) are assigned to Fe $2p_{3/2}$ and Fe $2p_{1/2}$, respectively, which are typical values of Fe^{3+}. The peaks of the Ni 2p at 856 and 873 eV are attributed to Ni $p_{3/2}$ and Ni $2p_{1/2}$ (Fig. 3C), respectively, corresponding to Ni^{2+}.[17] As for the O 1s region (Fig. 3D), the peaks locating at 532.6 and 531.1 eV are corresponding to the oxygen atoms from adsorbed water on the surface and the OH groups, another peak at 529.4 eV relates to the oxygen in metal–O bonds.[21]

The linear scanning voltammetries were carried out to evaluate the OER activity in alkaline solutions. As presented in Fig. 4, NiFe LDH/CuO NS behaves much better OER activity than others (Fig. 4A). NiFe LDH/CuO NS merely requires an overpotential of 270 mV to achieve the current density of 20 mA cm^{-2}, which is much lower than NiFe LDH/CuNWs (310 mV) and commercial RuO_2 (330 mV), respectively. CuO NS/CuNWs show negligible activity, implying that CuO NS has very low inherent OER activity, and NiFe LDH is mainly responsible for the excellent performance. The high OER activity of NiFe LDH/CuO NS continues with the potential going up. The overpotential at 50 mA cm^{-2} is 340 mV, still lower than 410 mV of RuO_2. In contrast, the OER activity of NiFe LDH/CuNWs increases slowly at potentials above 1.55 V. The high activity of NiFe LDH/CuO NS lies on the high density of NiFe LDH relative to NiFe LDH/CuNWs. CuO nanosheets, as nano-sized substrates, greatly increase the density of NiFe LDH. NiFe LDH/CuNWs with different NiFe dosages were also prepared and used for activity comparison. As presented in Fig. S4,† NiFe

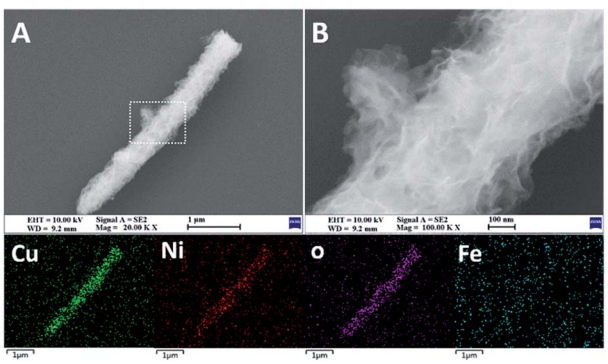

Fig. 2 High (A) and low (B) SEM images of NiFe LDH/CuO NS, and the EDS mapping of Cu, Ni, O, and Fe elements.

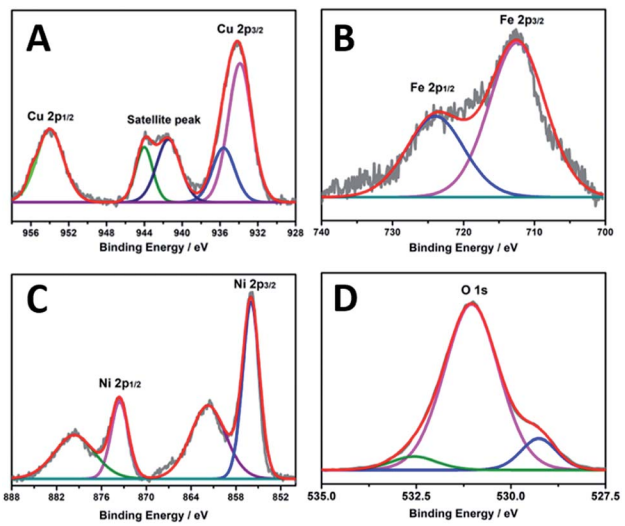

Fig. 3 XPS analysis of Cu 2p (A), Fe 2p (B), Ni 2p (C), and O 1s (D) orbitals of NiFe LDH/CuO NS.

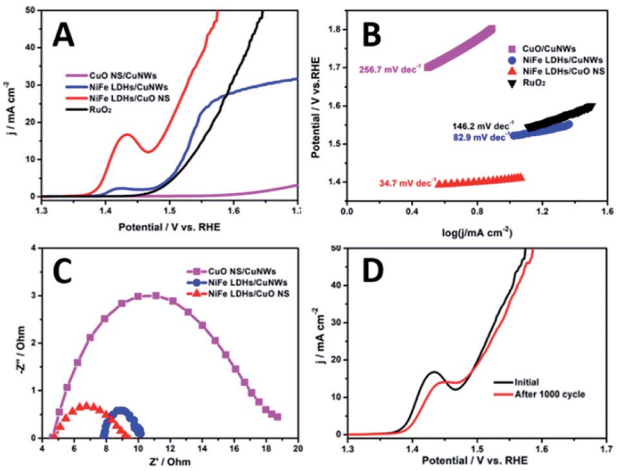

Fig. 4 Polarization curves (A) and Tafel plots (B) of CuO NS/CuNWs, NiFe LDH/CuNWs, NiFe LDH/CuO NS, and RuO_2 in 1 M KOH at the scanning rate of 5 mV s^{-1}; Nyquist plots of CuO NS/CuNWs, NiFe LDH/CuNWs, and NiFe LDH/CuO NS (C); the polarization curves of NiFe LDH/CuO NS before and after 1000 cycles of CV (D).

LDH/CuNWs performs higher activity than NiFe LDH/CuNWs-L and NiFe LDH/CuNWs-H, but they are still better than RuO_2. For low dosages of Ni and Fe, both the size and the density of NiFe LDH decrease, leading to the low OER activity. While for the large size of NiFe LDH and NiFe LDH/CuNWs-H, it decreases the active sites as well, hence leading to the poor OER activity.[22] The peaks located at $\approx$1.43 V (*vs.* RHE) corresponded to the oxidation of M(II) to M(III or IV) (M = Ni and Fe), which is common observed during the electrochemical process of Ni-based electrocatalysts.[23,24]

The Tafel plots were used to unravel the intrinsic OER activity of NiFe LDF/CuO NS catalysts. As exhibited in Fig. 4B, the Tafel slope of NiFe LDH/CuO NS is 34.7 mV dec^{-1}, which is smaller than that of RuO_2 (142.6 mV dec^{-1}), indicating the much more favourable catalytic kinetics.[25] NiFe LDH/CuNWs and CuO NS/CuNWs show the slopes of 82.9 and 256.7 mV dec^{-1}, respectively. The great gap in the slop between NiFe based catalysts and CuO NS/CuNWs confirms the main responsibility of NiFe LDH for the OER activity. NiFe LDF/CuO NS shows the good activity even compared to catalysts reported in literatures (Table S2†).

Nyquist plots obtained by electrochemical impedance spectroscopy (EIS) were used to investigate the charge-transfer process. As shown in Fig. 4C, the smallest R_{ct} is found on NiFe LDH/CuNWs, due to the excellent conductivity of CuNWs. Both NiFe LDH/CuNWs and NiFe LDFs/CuO NS have smaller R_{ct} than CuO NS/CuNWs, underlying the better conductivity of NiFe LDH than CuO NS. Generally, the small R_{ct} of NiFe LDF/CuO NS indicates the fast charge transfer, attributing to the improved conductivity and surface adsorption ability.[26] NiFe LDF/CuO NS shows the highest OER activity but lower conductivity than NiFe LDH/CuNWs, which evidences that increasing the active sites is more important than improving the conductivity.

The durability was also examined by evaluating the HER activity after 1000 cycles of continuous CV. As shown in Fig. 4D, small decays are shown at high current densities. The overpotential at 50 mA cm^{-2} is 340 mV, only a 10 mV decay is present.

In summary, NiFe LDFs/CuO NS performs high activity towards OER. The CuO nanosheets, as nano-sized substrates, are crucial to downsize NiFe LDH. As a result, the amount of active sites for OER is greatly increased. Compared with the effect of conductivity, the structure engineering plays a larger role in the OER activity. This sheet-on-sheets strategy is proven to be effective for boosting the active sites and hence, enhancing the OER activity. Undoubtedly, this work provides a facile method to synthesize the nanoscale substrate, which will greatly reduce the size of LDH.

Conflicts of interest

There are no conflicts to declare.

Acknowledgements

This research was supported by National Natural Science Foundation of China (No. 21606049).

Notes and references

1 L. Zhong, Y. Bao, X. Yu and L. Feng, *Chem. Commun.*, 2019, **55**, 9347–9350.
2 M. Laipan, J. Yu, R. Zhu, J. Zhu, A. T. Smith, H. He, D. O'Hare and L. Sun, *Mater. Horiz.*, 2020, **7**, 715–745.
3 Y. Zheng, B. Cheng, W. You, J. Yu and W. Ho, *J. Hazard. Mater.*, 2019, **369**, 214–225.
4 X. Li, M. Fan, D. Wei, X. Wang and Y. Wang, *J. Electrochem. Soc.*, 2020, **167**, 024501.
5 A. Grimaud, O. Diaz-Morales, B. Han, W. T. Hong, Y. L. Lee, L. Giordano, K. A. Stoerzinger, M. T. M. Koper and Y. Shao-Horn, *Nat. Chem.*, 2017, **9**, 457–465.
6 Z. Li, S. Wang, Y. Tian, B. Li, H. J. Yan, S. Zhang, Z. Liu, Q. Zhang, Y. Lin and L. Chen, *Chem. Commun.*, 2020, **56**, 1749–1752.
7 J. M. P. Martirez and E. A. Carter, *J. Am. Chem. Soc.*, 2019, **141**, 693–705.
8 R. Li, Y. Wang, W. Li, S. Zhou, P. Tian, H. Gao, X. Liu and J. Zang, *Chem. Commun.*, 2019, **55**, 13370–13373.
9 Z. Xue, X. Zhang, J. Qin and R. Liu, *J. Mater. Chem. A*, 2019, **7**, 23091–23097.
10 A. Bähr, G.-h. Moon and H. Tüysüz, *ACS Appl. Energy Mater.*, 2019, **2**, 6672–6680.
11 Y. Li, L. Hu, W. Zheng, X. Peng, M. Liu, P. K. Chu and L. Y. S. Lee, *Nano Energy*, 2018, **52**, 360–368.
12 Z. Lu, W. Xu, W. Zhu, Q. Yang, X. Lei, J. Liu, Y. Li, X. Sun and X. Duan, *Chem. Commun.*, 2014, **50**, 6479–6482.
13 S. Chen, J. Duan, P. Bian, Y. Tang, R. Zheng and S.-Z. Qiao, *Adv. Energy Mater.*, 2015, **5**, 1500936.
14 F. Lu, M. Zhou, Y. Zhou and X. Zeng, *Small*, 2017, **13**, 1701931.

15 W. Wang, Y. Liu, J. Li, J. Luo, L. Fu and S. Chen, *J. Mater. Chem. A*, 2018, **6**, 14299–14306.
16 L. Yang, H. Liu, H. Shen, Y. Huang, S. Wang, L. Zheng and D. Cao, *Adv. Funct. Mater.*, 2020, **30**, 1909889.
17 B. Zhu, Q. Hu, X. Liu, G. Li, L. Fan, Q. Zhang, J. Liu and C. He, *Chem. Commun.*, 2018, **54**, 10187–10190.
18 Q. Zhou, T.-T. Li, J. Qian, W. Xu, Y. Hu and Y.-Q. Zheng, *ACS Appl. Energy Mater.*, 2018, **1**, 1364–1373.
19 H. Zhang, X. Li, A. Hähnel, V. Naumann, C. Lin, S. Azimi, S. L. Schweizer, A. W. Maijenburg and R. B. Wehrspohn, *Adv. Funct. Mater.*, 2018, **28**, 1706847.
20 A. A. Dubale, A. G. Tamirat, H.-M. Chen, T. A. Berhe, C.-J. Pan, W.-N. Su and B.-J. Hwang, *J. Mater. Chem. A*, 2016, **4**, 2205–2216.
21 Z. Sun, Y. Wang, L. Lin, M. Yuan, H. Jiang, R. Long, S. Ge, C. Nan, H. Li, G. Sun and X. Yang, *Chem. Commun.*, 2019, **55**, 1334–1337.
22 C. Roy, B. Sebok, S. B. Scott, E. M. Fiordaliso, J. E. Sørensen, A. Bodin, D. B. Trimarco, C. D. Damsgaard, P. C. K. Vesborg, O. Hansen, I. E. L. Stephens, J. Kibsgaard and I. Chorkendorff, *Nat. Catal.*, 2018, **1**, 820–829.
23 H. Xu, Z. X. Shi, Y. X. Tong and G. R. Li, *Adv. Mater.*, 2018, **30**, e1705442.
24 X. Zhao, X. Ding, Y. Xia, X. Jiao and D. Chen, *ACS Appl. Nano Mater.*, 2018, **1**, 1476–1483.
25 J. Jiang, L. Chang, W. Zhao, Q. Tian and Q. Xu, *Chem. Commun.*, 2019, **55**, 10174–10177.
26 M. Y. Ye, S. Li, X. Zhao, N. V. Tarakina, C. Teutloff, W. Y. Chow, R. Bittl and A. Thomas, *Adv. Mater.*, 2020, e1903942, DOI: 10.1002/adma.201903942.